# Synthesis and evaluation of *N*,*N*′-((2*R*,2′*R*)-(succinylbis(oxy))bis(2-hydroxypropane-3,1-diyl))bis(*N*,*N*-dimethyltetradecan-1-aminium)dibromide as an inhibitor against carbon steel corrosion: implementation of adsorption methodology using Fermi energy and Monte Carlo simulation

**M.J. Meften***

*Department of Chemistry, College of Education-Qurna, University of Basrah, Basra 61001, Iraq*
**E-mail: mushtaq.meften@uobasrah.edu.iq*

## Abstract

*N*,*N*′-((2*R*,2′*R*)-(Succinylbis(oxy))bis(2-hydroxypropane-3,1-diyl))bis(*N*,*N*-dimethyltetradecan-1-aminium)dibromide (SHBA) was prepared, tested, and evaluated as an inhibitor for N-80 carbon steel used in oil and gas transmission and down-hole pipelines. It was tested in a 0.5 mol·L$^{-1}$ HCl solution at 30°C (±2). The SHBA was assessed as an inhibitor using potentiodynamic polarization (PP), electrochemical impedance spectroscopy (EIS), and scanning electron microscopy-energy dispersive X-ray spectroscopy (SEM/EDX). The compound SHBA acts as a mixed-type inhibitor, as shown by EIS and PP results. It demonstrates excellent performance with maximum efficiencies of 93.63% and 93.04%, respectively. The EDX analysis showed an efficiency of 95.38%. The Monte Carlo method was used to determine the adsorption sites of SHBA on the carbon steel surface. MC explained the adsorption of oxygen and nitrogen atoms on the Fe (111) surface, confirming SHBA's strong adsorption. The *HOMO* energy of SHBA is –6.022 eV, which is higher than the Fermi level energy of –0.8756 Ha (–28.188 eV), indicating stable adsorption. Metallic features were observed in SHBA from the maximum valence band and minimum conduction band. The electrostatic potential surface (EPS) and electronic characteristics of SHBA were studied. Theoretical results agree with the experimental findings.

Received: November 28, 2025. Published: March 11, 2026 doi: 10.17675/2305-6894-2026-15-1-23

***Keywords:*** *corrosion inhibitors, EIS, Fermi energy, adsorption methodology, SEM/EDX, Monte Carlo, Tafel plot.*

## 1. Introduction

Corrosion causes significant economic losses and threatens the national economy. Various strategies to combat corrosion include the use of corrosion inhibitors, coatings, and cathodic protection [1]. Molecules with polar functional groups such as –CHO, –$NO_2$, –CN, –$NH_2$, –OH, –SH, π-electrons, aromatic rings, and heteroatoms like oxygen, sulfur, nitrogen, and phosphorus, whether in rings or side chains, are highly effective as corrosion inhibitors.

These molecules adsorb onto surfaces, reducing metal dissolution and forming protective films that shield metal from corrosive media [2, 3]. In the *ex-situ* petroleum process, carbon steel commonly used in pipes and tubing rusts significantly due to the acidic solution. Inhibitors are mixed with the acidic solution before the pickling process to reduce metal corrosion. Theoretical studies help determine the electronic properties of inhibitors [4], clarifying corrosion mechanisms by quantitative calculations of how inhibitors react with metal surfaces. These methods evaluate the electronic properties and geometry of inhibitor molecules [5], aiding in the development of more effective corrosion inhibitors [6]. Since conventional inhibitors like chromates are hazardous, organic inhibitors are increasingly preferred as safer alternatives, leading to widespread use of corrosion inhibitors [7]. Fermi levels and Monte Carlo simulations are essential for identifying reactive sites on inhibitor molecules for optimal adsorption on metal surfaces [8]. Characteristics such as the *LUMO*, *HOMO*, hardness, softness, electronic energy, solvation energy, potential energy, and electron transfer capacity strongly influence a molecule's ability to interact. Recently, compounds with phenyl rings and heteroatom aromatic systems have been used effectively as corrosion inhibitors [9–11]. In a similar previous study, the inhibition efficiency of *N*,*N*′-((1,4-phenylenebis(azanediyl))bis(2-hydroxypropane-3,1-diyl))bis(*N*,*N*-dimethyldecan-1-aminium) is 87.17% and was very close to our research results, 92.05% [12]. Also, a series of quaternary ammoniums to hexanediyl-1,6-bis-(diethyl alkyl ammonium bromide) were evaluated as inhibitors in 1M HCl; the results showed that the inhibitors were excellent [13]. Also, in a previous study, the inhibition efficiency of sodium 2,2′-(18,25-dioxo-17,26-dioxa-20,23-diazadotetracontane-20,23-diyl) diacetate is excellent [3]. This paper primarily aims to examine and evaluate *N*,*N*′-((2*R*,2′*R*)-(succinylbis(oxy))bis(2-hydroxypropane-3,1-diyl))bis(*N*,*N*-dimethyltetradecan-1-aminium)dibromide (SHBA) as an effective, low-cost, and highly efficient corrosion inhibitor. It is used to protect water treatment plants, downhole pipelines, petroleum flow lines, and crude oil pipelines. Electrochemical methods, including Tafel plots, EDX, and EIS, as well as theoretical approaches such as the Fermi energy Monte Carlo simulations and electrostatic potential surface analysis, were employed to assess the SHBA inhibitor.

## 2. Experimental and Theoretical Details

### *2.1. Experimental specifications*

The EIS tests were conducted at 30°C in a 0.5 $mol \cdot L^{-1}$ HCl solution as the corrosion medium, with the SHBA inhibitor at concentrations of 0.01, 0.02, 0.03, 0.04, and 0.05 $mol \cdot L^{-1}$. Carbon steel N-80, used in various applications such as transmission pipelines, downhole tubulars, and petroleum flow lines, has a chemical composition including 0.31% carbon, 0.92% manganese, 0.20% chromium, 0.01% phosphorus, 0.008% sulfur, 0.19% silicon, and 98.362% iron [14]. For potentiodynamic polarization (PP) and EIS measurements, the carbon steel was cut into 0.5 cm thick, 1 cm in diameter pieces. The polarization curves were recorded using a CHI660B/400S instrument. The open circuit

potential (OCP) was monitored over a 6-minute scan at a rate of 0.8 mV/s. Polarization potentials ranging from −250 mV to +250 mV were applied to obtain typical Tafel curves. Impedance data were collected with the device software CHI660D, recording impedance curves at OCP with a 10 mV peak-to-peak amplitude across a frequency range from 1000 Hz to 100 Hz. The electrochemical cell used for PP and EIS techniques had a volume of 250 mL. It included three electrodes: the platinum as the auxiliary electrode, a standard calomel electrode (SCE) as the reference, and carbon steel as the working electrode.

### *2.2. Synthesis of N,N'-((2R,2'R)-(succinylbis(oxy))bis(2-hydroxypropane-3,1-diyl))bis(N,N-dimethyl tetradecan-1-aminium)dibromide (SHBA) [15]*

**Step 1:** Synthesis of bis(3-chloro-2-hydroxypropyl) succinate (ES).

Tetra-*n*-butyl ammonium iodide (0.2 g, 0.0005 mol) and succinic acid (2.36 g, 0.02 mol) were mixed with epichlorohydrin (47.1 mL, 0.06 mol). After five hours of refluxing and stirring, the mixture yielded 4.54 g of light orange oil (74.9% yield) of the target compound (ES).

**Step 2:** Synthesis of bis(3-(dimethyl amino)-2-hydroxypropyl) succinate (2ES).

To a flask containing 0.67 g (0.012 mol) of KOH was added 2.7 mL (0.02 mol) of 33% aqueous dimethylamine. Then, 3.03 g (0.01 mol) of the compound (ES) was added dropwise and stirred at room temperature to produce a precipitate. The mixture was filtered, and the filtrate was extracted with chloroform, then dried over anhydrous magnesium sulfate. The solvent was removed by evaporation, yielding 2.13 g of the target compound (2ES) as a dark orange oil.

**Step 3:** Synthesis of *N*,*N*′-((2*R*,2′*R*)-(succinylbis(oxy))bis(2-hydroxypropane-3,1-diyl))-bis(*N*,*N*-dimethyl tetradecan-1-aminium)dibromide (SHBA).

To a flask containing 1.86 mL (0.00626 mol) of 1-bromotetradecane and 50 mL of absolute isopropyl alcohol was added 1.0 g, 0.00313 mol of the compound (2ES) at room temperature. The mixture was refluxed for 1 hour. After the reaction was complete, the mixture was evaporated, and the residue was purified by column chromatography on silica gel using a chloroform/ethyl acetate mixture (1:2 v/v), yielding 2.06 g of the target compound as an orange oil (75.4% yield) [15]. The schematic structure of SHBA is shown in Figure 1. The preparation mechanism is shown in Scheme 1.

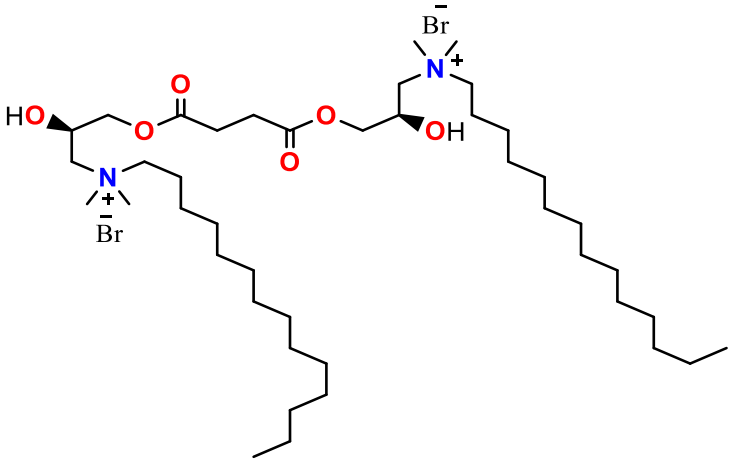

**Figure 1.** Schematic structure of SHBA inhibitor.

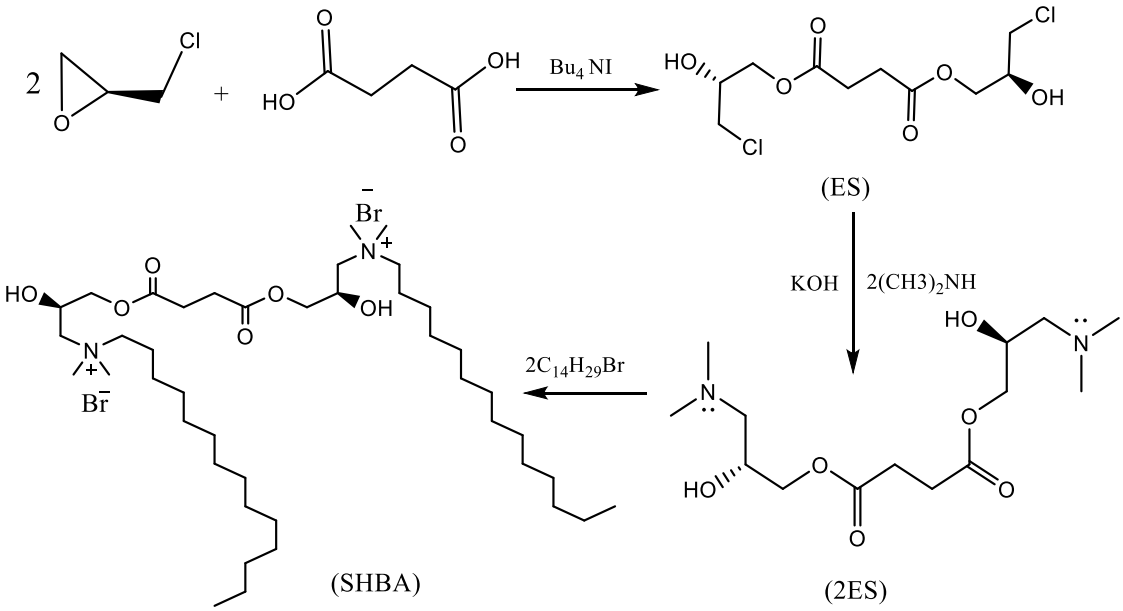


**Scheme 1.** Synthesis mechanism of SHBA.

### *2.3. Methodology of practical calculations*

Equations 1, 2, and 3 have been used in EIS experiments to determine Randle's circuit inhibition efficiency ($E_I$), surface coverage ($S_c$), and double-layer capacitance ($C_{dl}$), where $R_{ct(free)}$, $R_{ct(inh)}$, and ($f_{max}$) are the charge transfer resistances in the absence and presence of an inhibitor, and the maximum frequency, respectively [16]. Equation 4 was used to determine the time constant ($\tau$) of the charge-transfer process [17]. Equation 5 calculates the excess positive potential ($E_{PP}$) on the surface, known as Andropov's rational corrosion potential [18]. The open-circuit potential is labeled as ($E_{OCP}$), and the potential of zero charge as ($E_{PZC}$). At low frequencies, the fitted semicircle intersects the real axis ($Z_{real}$) to determine the charge transfer resistance ($R_{ct}$). At high frequencies, the semicircle's intersection with

the real axis ($Z_{real}$) was used to estimate the solution resistance ($R_s$). Equation 6 was employed to calculate $R'_{ct}$, which considers both the charge transfer and resistance of the diffusion layer at the working electrode [19].

$$E_I(\%) = \left(1 - \frac{R_{ct(free)}}{R_{ct(inh)}}\right) \cdot 100 \quad (1)$$

$$S_c = \left(1 - \frac{R_{ct(free)}}{R_{ct(inh)}}\right) \quad (2)$$

$$C_{dl} = \left(\frac{1}{2\pi f_{max} R_{ct}}\right) \quad (3)$$

$$\tau = C_{dl} R_{ct} \quad (4)$$

$$E_{PP} = E_{OCP} - E_{PZC} \quad (5)$$

$$R'_{ct} = R_{ct} - R_s \quad (6)$$

The corrosion current density ($i_{corr}$) was identified as a characteristic of the PP method. Equation 7 was used to calculate the inhibition efficiency in the polarization study, where $i^0_{cor}$ and $i^{in}_{cor}$ represent the corrosion current densities without and with the SHBA inhibitor, respectively [20]. Equation 8 was employed to determine the potential displacement $\Delta E_{corr}$, where $E^{in}_{cor}$ and $E^0_{cor}$ denote the corrosion potentials in the presence and absence of an SHBA, respectively [21].

$$IE(\%) = \frac{i^0_{cor} - i^{in}_{cor}}{i^0_{cor}} \quad (7)$$

$$\Delta E_{cor} = E^{in}_{cor} - E^0_{cor} \quad (8)$$

The INCA 400 device was used to record EDX spectra of carbon steel in the presence and absence of SHBA at a voltage of 10 kV. Equation 9 was applied to determine the proportion of corroded iron, where $\%E^0$ and $\%E$ represent the percentage of iron in reference carbon steel and the percentage of iron after corrosion, respectively. The inhibition efficiency ($IE\%$) was calculated using Equation 10, where $\%Fe_{loss}$ and $\%Fe''_{loss}$ represent the percentage of corroded iron with and without SHBA, respectively [22, 1].

$$Corroded\ iron(\%) = \frac{\%E^0 - \%E}{\%E^0} \cdot 100 \quad (9)$$

$$IE(\%) = \frac{\%Fe''_{loss} - \%Fe_{loss}}{\%Fe''_{loss}} \cdot 100 \quad (10)$$

Inhibition efficiency of SHBA by the weight loss method was measured at the periods of time 1, 3, and 6 hours, at 30, and 70°C. Inhibition efficiency and surface coverage (θ) were calculated by Equations 11 and 12, respectively [12].

$$IE(\%) = \frac{w_1 - w_2}{w_1} \cdot 100 \tag{11}$$

$$\theta = \frac{w_1 - w_2}{w_1} \tag{12}$$

### *2.4. Methodology of theoretical calculations*

To analyze the properties of the SHBA compound, the DMol3/EPS software was used to interpret its adsorption on the iron surface and provide key information on its inhibition mechanisms. Equation 13 shows the ionization energy (*IE*) [23], and the $\Delta E_{\text{back-donation}}$ was calculated using Equation 14 [24]. Monte Carlo (MC) simulations and the Fermi energy were studied to understand the adsorption process and identify the most stable interaction sites [25]. For the MC simulations, a size of 28.28 Å×28.28 Å×10.12 Å for Fe (111) was used, along with a 35 Å layer along the x-axis. Equations 15, 16, 17, and 18 were used to calculate the softness (*s*), hardness (η), energy gap (Δ*E*), and electronegativity (χ), respectively [11, 26].

$$I_{\text{E}} = -E_{\text{HOMO}} \tag{13}$$

$$\Delta E_{\text{black-donation}} = -\frac{\eta}{4} \tag{14}$$

$$s = \frac{1}{\eta} \tag{15}$$

$$\eta = \frac{\Delta E_{\text{gap}}}{2} \tag{16}$$

$$\Delta E_{\text{gap}} = E_{\text{LUMO}} - E_{\text{HOMO}} \tag{17}$$

$$\chi = \frac{(-E_{\text{HOMO}}) + (-E_{\text{LUMO}})}{2} \tag{18}$$

## 3. Results and Discussion

### *3.1. Results of the electrochemical impedance spectroscopy (EIS)*

The SHBA compound was specifically tested as a corrosion inhibitor using EIS. The loop capacitance is higher at all inhibitor concentrations than without it, as shown in Figure 2a. This suggests that SHBA enhances the resistance of carbon steel against corrosion due to surface uniformity and stable frequency. In the Nyquist plot, the semicircles are nearly

complete [27, 28]. As SHBA concentration increases, the semicircle diameter grows, indicating a lower corrosion rate and improved adsorption efficiency. High semicircular arcs are visible at all frequencies [29, 30], with the highest efficiency at the lowest frequency, 28.82 Hz, reaching 93.63%, which indicates better corrosion inhibition (Figure 2c). The effectiveness of SHBA significantly increases at lower frequencies [31]. At all tested concentrations, 0.05 M provided the highest resistance. These results confirm optimal inhibition; Figure 2a displays all data [32]. As SHBA concentration increased, the charge transfer resistance $R_{ct}$ increased significantly, reaching 307.26 $\Omega \cdot cm^2$, as shown in Table 1. These findings suggest that a protective layer forms on the carbon-steel surface, inhibiting corrosion and acting as a barrier to charge transfer [30, 32]. Conversely, the noticeable decrease in double-layer capacitance results from SHBA adsorption onto the carbon steel surface, which decreases the local dielectric constant, increases the adsorbed film thickness, or both. This can be explained by the gradual displacement of water molecules on the carbon steel surface by adsorbed SHBA molecules, which possess a lower dielectric constant [1, 33]. The decrease in both $C_{dl}$ and $f_{max}$, alongside the steady increase in $\tau$ and $R_{ct}$, suggests that SHBA molecules adsorbed evenly on the N-80 surface [1]. The potential of zero charge (PZC) is significant in surface science because it signifies a surface with zero electric charge density and is closely related to adsorption. The PZC allows calculation of the metal's surface charge based on the open-circuit potential (OCP). Electrochemical impedance measurements determined this at various potentials; Figure 2b shows the plot of $C_{dl}$ *versus* applied potential. The applied potential was measured at 88.8 mV relative to the minimum of $C_{dl}$, which can be considered the potential of zero charge for iron without SHBA, whereas it was 105.4 mV at 0.05 M of SHBA. The open-circuit potential was 157.5 mV/SCE in the presence of the inhibitor, compared to 125.7 mV without it, as shown in Figure 2b. Since the OCP values are higher than the PZC, the N-80 surface charge ($E_{PP}$) is positive at +36.9 mV and +52.1 mV, indicating a positively charged carbon steel surface. Due to the anodic dissolution of metal, the carbon steel surface acquires a positive charge, so $Cl^-$ ions are likely to be adsorbed first. Under these conditions, the SHBA molecule is protonated in an acid medium and adsorbs onto the surface through electrostatic interactions. Alternatively, the SHBA molecules may adsorb onto the Fe surface via lone pairs of electrons on the O atoms [1, 34].

Figure 3a shows the simple Nyquist plot, and Figure 3b displays the electrochemical equivalent circuit used to fit the EIS plots. The $R_\Omega$=series resistance, $R'_{ct} = R_{ct} - R_s$, $w = Z''/(Z' - R_\Omega) \cdot R_{ct} \cdot C_{dl}$ (Warburg impedance). Consequently, the real and imaginary components of cell impedance are $Z' = R_\Omega + R_{ct}/(1 + w^2 \cdot C_{dl}^2 \cdot R_{ct}^2)$ and $Z'' = w \cdot C_{dl} \cdot R_{ct}^2/(1 + w^2 \cdot C_{dl}^2 \cdot R_{ct}^2)$, respectively. The equation of a semicircle ($Z''$ *vs.* $Z'$) has its center on the $Z'$ axis at $Z' = R_\Omega + 1/2 \cdot R_{ct}$ and radius $1/2 \cdot R_{ct}$. The interaction with the $Z'$ axis is at $Z' = R_\Omega$ for $w = \infty$ and at $Z' = R_\Omega + R_{ct}$ when $w = 0$. This is referred to as the Nyquist plot [35].

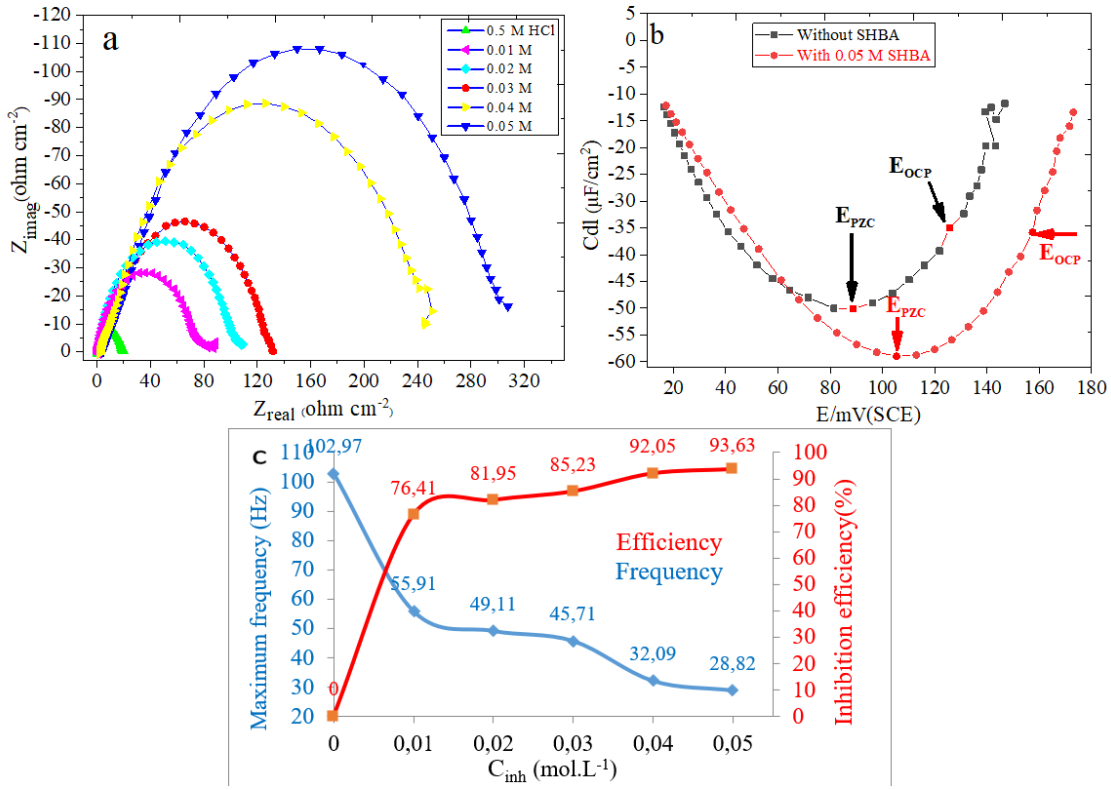


**Figure 2.** (a) Typical Nyquist plots of SHBA, (b) plots of $C_{dl}$ *vs.* applied potential, and (c) SHBA concentration effect on the frequency and inhibition efficiency.

**Table 1.** Results of SHBA inhibitor *via* EIS technique at 30°C (±2).

| Conc., mol·L$^{-1}$ | $f_{max}$, Hz | $C_{dl}$, µF·cm$^{-2}$ | $R_{ct}$, Ω·cm$^2$ | $R_s$, Ω·cm$^2$ | $R'_{ct}$, Ω·cm$^2$ | $E_I$, % | $S_c$ | τ, sec | $E_{OC}$, mV | $E_{PZ}$, mV | $E_{pp}$, mV |
|---|---|---|---|---|---|---|---|---|---|---|---|
| 0.00 | 102.97 | 79.10 | 19.55 | 0.14 | 19.41 | – | – | 0.0015 | 125.7 | 88.8 | 36.9 (+) |
| 0.01 | 55.91 | 34.36 | 82.88 | 0.23 | 82.65 | 76.41 | 0.764 | 0.0028 | – | – | – |
| 0.02 | 49.11 | 29.93 | 108.32 | 1.02 | 107.30 | 81.95 | 0.819 | 0.0032 | – | – | – |
| 0.03 | 45.71 | 26.30 | 132.43 | 1.33 | 131.10 | 85.23 | 0.852 | 0.0034 | – | – | – |
| 0.04 | 32.09 | 20.17 | 245.92 | 1.20 | 244.72 | 92.05 | 0.920 | 0.0049 | – | – | – |
| 0.05 | 28.82 | 17.98 | 307.26 | 1.25 | 306.01 | 93.63 | 0.936 | 0.0055 | 157.5 | 105.4 | 52.1 (+) |

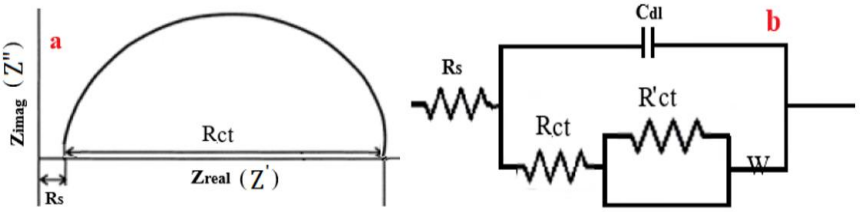


**Figure 3.** (a) Simple Nyquist plot, and (b) the electrochemical equivalent circuit used to fit the EIS plots.

### *3.2. Results analysis of potentiodynamic polarization (PP)*

The potentiodynamic polarization curves of carbon steel corrosion in 0.5 M HCl at various SHBA inhibitor doses are shown in Figure 4a. These curves demonstrate that the adsorption of SHBA molecules on the carbon steel surface decreases the corrosion current density as the inhibitor concentration increases. Consequently, this reduces the N-80 dissolution rate because the surface becomes covered, blocking access for corrosive agents [36, 37]. Additionally, at all tested concentrations, the corrosion current density was substantially lower than in the absence of the inhibitor, likely because SHBA molecules adhered to the N-80 surface, blocking its active sites [38]. The interaction of the SHBA inhibitor on the carbon steel surface enhances inhibition efficiency. Table 2 shows that as SHBA concentration increases, surface coverage ($S_c$) of N-80 also increases, reaching 93.04% inhibition efficiency at the optimal dose of 0.05 M [37]. If the shift in corrosion potential exceeds 85 mV compared to the potential without an inhibitor, it indicates an anodic or cathodic inhibitor. Whereas if it is less than 85 mV, it is a mixed inhibitor. Since the maximum potential shift observed is 29 mV at 0.02 M of SHBA, which is less than 85 mV, SHBA acts as a mixed-type inhibitor, simultaneously inhibiting both cathodic and anodic processes. All results are shown in Table 2 and Figure 4b [36–39]. The effect of concentration on $\Delta E_{corr}$ values shows a trend toward the anodic zone at all concentrations except 0.01 M, which shifts toward the cathodic zone by –4 mV, as shown in Figure 5a [21]. Figure 5b shows that the efficiency increases and the corrosion current density decreases as the SHBA concentration rises.

**Table 2.** Results of SHBA inhibitor by PP method at 30°C (±2).

| **Conc., mol·L$^{-1}$** | **$E_{corr}$, mV/SCE** | **$i_{corr}$, mA·cm$^{-2}$** | **$\Delta E_{corr}$, mV** | **$S_c$** | **%*IE*** |
|---|---|---|---|---|---|
| 0.00 | –322 | 65.11 | – | – | – |
| 0.01 | –326 | 14.91 | –4 | 0.7710 | 77.10 |
| 0.02 | –293 | 10.34 | 29 | 0.8411 | 84.11 |
| 0.03 | –318 | 7.98 | 4 | 0.8774 | 87.74 |
| 0.04 | –317 | 5.77 | 5 | 0.9113 | 91.13 |
| 0.05 | –309 | 4.53 | 13 | 0.9304 | 93.04 |

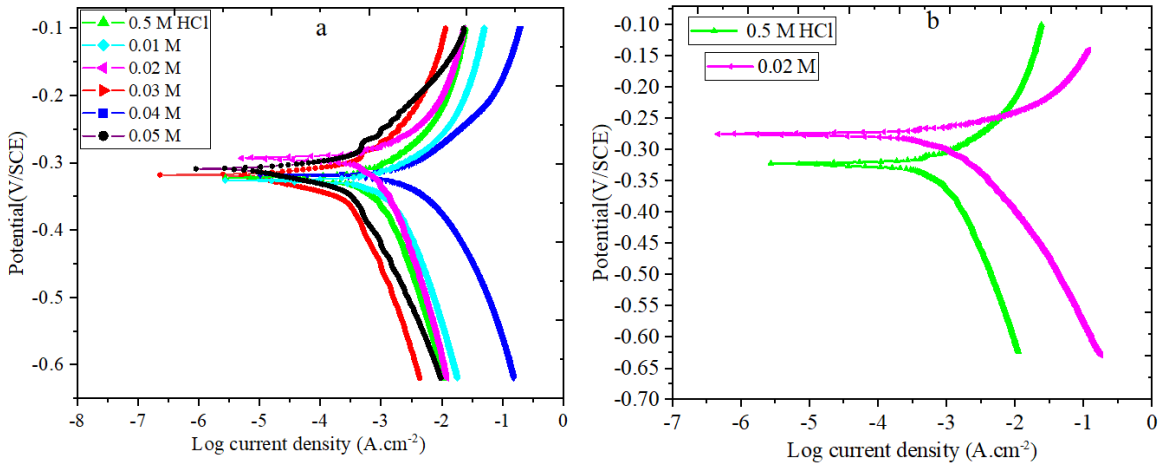


**Figure 4.** (a) Typical Tafel plots of the SHBA inhibitor by the PP method, and (b) maximal shift of corrosion potential.

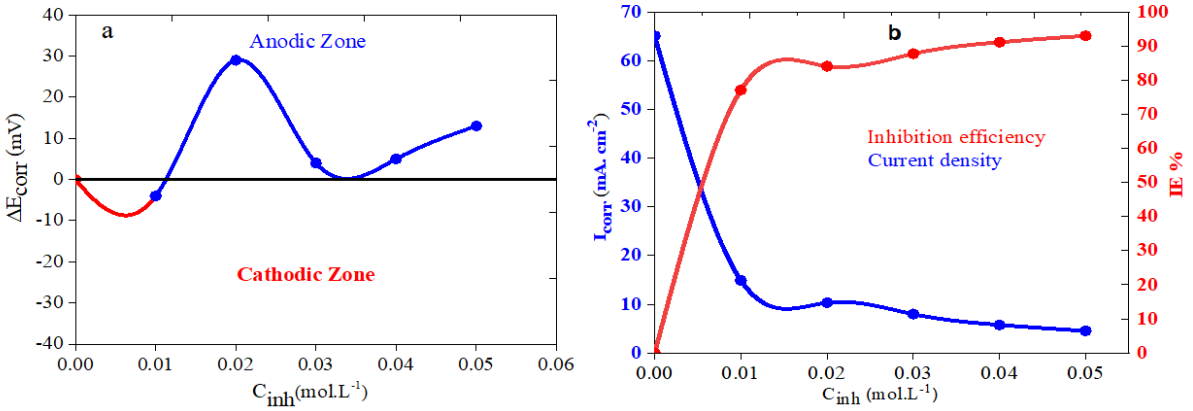


**Figure 5.** (a) Concentration effect on $\Delta E_{corr}$ (anodic and cathodic zones), (b) Concentration effect on the inhibition and current density.

### *3.3. Results of SEM/EDX*

The EDX technique was used to determine element percentages, inhibitor efficiency of SHBA, and the corrosion rate of iron after immersion in 0.5 mol·L$^{-1}$ HCl for 5 hours. To verify the EDX results, experiments were conducted at an optimal SHBA concentration of 0.05 mol·L$^{-1}$. Figure 6a shows the EDX spectra for the carbon steel reference, highlighting peaks for the major elements, iron, oxygen, and carbon, with iron comprising a high proportion of 98.362%. After immersion in 0.5 mol·L$^{-1}$ HCl without SHBA, a significant reduction in iron content of the carbon steel to 77.29% was observed, as shown in Figure 6b. Meanwhile, the proportions of C and O increased to 20.95% and 12.02%, respectively, indicating the formation of corrosion products. This confirms that without SHBA, carbon steel was corroded, leaving its surface unprotected [1, 22, 40]. The EDX spectrum of N-80 after immersion in 0.5 mol·L$^{-1}$ HCl containing 0.05 mol·L$^{-1}$ of SHBA inhibitor is shown in

Figure 6c, where slight corrosion was observed, with an iron content of 97.39% and an inhibition efficiency of 95.38%, indicating the formation of a layer of SHBA molecules adsorbed onto the carbon steel surface, as listed in Table 3. The EDX analysis validated the electrochemical results obtained from the PP and EIS methods; the inhibition results were nearly identical [22, 40, 41]. The analysis of the N-80 surface was performed using scanning electron microscopy at an optimum concentration of 0.05 M for 5 hours. The surface after immersion with and without an inhibitor is shown in Figures 7a and 7b, respectively. SEM of the N-80 surface in the absence of SHBA showed the occurrence of regular corrosion pitting and noticeable distortions, while it was smoother and more even compared with the absence of SHBA. This indicates the occurrence of slight corrosion in the event of inhibitor presence [22].

**Table 3.** EDX results of the SHBA inhibitor at 0.05 mol·L$^{-1}$.

| Carbon steel (N-80) | Oxygen element, % | Carbon element, % | Iron element, % | Percentage of corroded iron, % | Inhibitor efficiency, % |
|---|---|---|---|---|---|
| Reference | 1.06 | 0.22 | 98.362 | – | – |
| With SHBA | 7.30 | 12.20 | 97.39 | 0.988 | 95.38 |
| 0.5 M HCl | 12.02 | 20.95 | 77.29 | 21.42 | – |

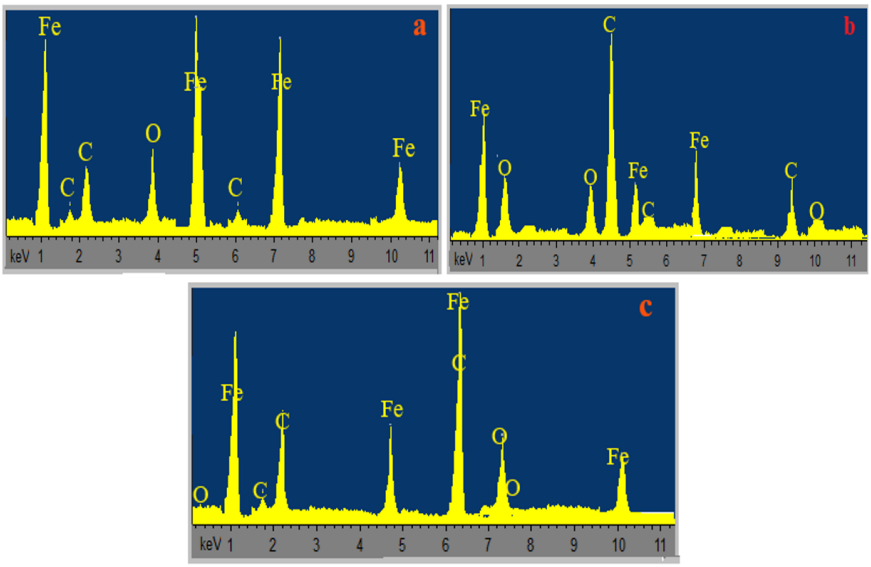


**Figure 6.** The EDX spectra of carbon steel: (a) polished (reference), (b) uninhibited carbon steel, and (c) inhibited carbon steel.

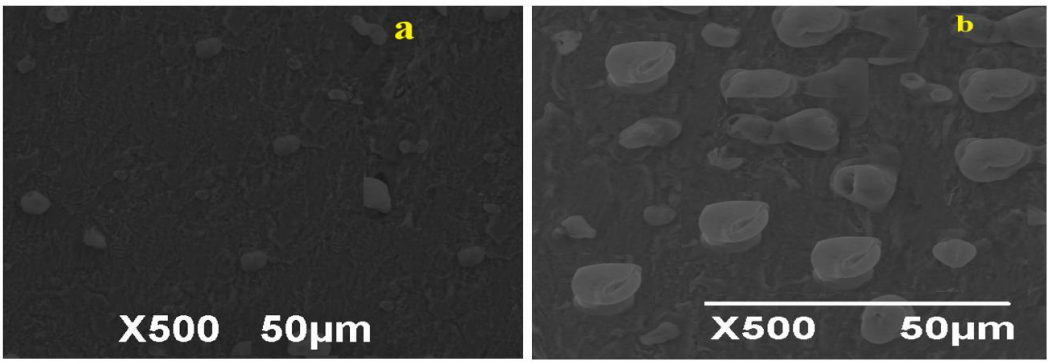


**Figure 7.** SEM images for N-80 surface, (a) with the presence of inhibitor, (b) in inhibitor absence.

### *3.4. The influence of temperature and time by weight loss method*

The weight loss method was used to determine the effect of time and temperature on inhibitor efficiency. From the results listed in Tables 4 and 5 and Figures 8 and 9, it was concluded that the weight loss was considerably decreased with concentration increase at a proven time due to the increased amount of inhibitor used, thereby increasing the surface area covered by inhibitor molecules. Also, it was observed that as the exposure time increased, the inhibition efficiency did not decrease significantly (slight decrease). This confirms the stability of the adsorption process of the inhibitor and the consistency of its efficiency. Subsequently, it can be concluded that the inhibitor has high efficiency due to its adsorption on the carbon steel surface through non-bonding electron pairs of oxygen atoms. The zwitterion can provide both physical and chemical adsorption. The SHBA has the hydrophilic part and the hydrophobic part. In this case, the hydrophobic part in inhibitor molecules will adsorb on the carbon steel surface and protect it. while the hydrophilic part prevents corrosive materials from the surface [12, 42]. Weight loss increases with temperature rise; hence, inhibition efficiency a little decrease with increasing the solution temperature. Inhibition efficiency decrease refers to the fact that the formed film on N-80 surface is less protective at high temperature because the desorption rate of the inhibitor is faster at high temperatures, and due to the removal of physical adsorption [12, 43, 44].

**Table 4.** Results of weight loss method at different times at 30±2°C.

| **Time** | **1 hr.** | | | **3 hrs.** | | | **6 hrs.** | | |
|---|---|---|---|---|---|---|---|---|---|
| **Conc., mol·L$^{-1}$** | ***WL*, mg** | **%*IE*** | **θ** | ***WL*, mg** | **%*IE*** | **θ** | ***WL*, mg** | **%*IE*** | **θ** |
| 0.5 HCl | 215 | – | – | 450 | – | – | 506 | – | – |
| 0.01 | 49 | 77.20 | 0.7720 | 127 | 71.77 | 0.7177 | 149 | 70.55 | 0.7055 |
| 0.02 | 38 | 82.32 | 0.8232 | 88 | 80.44 | 0.8044 | 109 | 78.45 | 0.7845 |

| Time | 1 hr. | | | 3 hrs. | | | 6 hrs. | | |
|---|---|---|---|---|---|---|---|---|---|
| **Conc., mol·L$^{-1}$** | ***WL*, mg** | **%*IE*** | **θ** | ***WL*, mg** | **%*IE*** | **θ** | ***WL*, mg** | **%*IE*** | **θ** |
| 0.03 | 32 | 85.11 | 0.8511 | 71 | 84.22 | 0.8422 | 93 | 81.62 | 0.8162 |
| 0.04 | 24 | 88.83 | 0.8883 | 59 | 86.88 | 0.8688 | 88 | 82.60 | 0.8260 |
| 0.05 | 20 | 90.69 | 0.9069 | 48 | 89.33 | 0.8933 | 60 | 88.14 | 0.8814 |

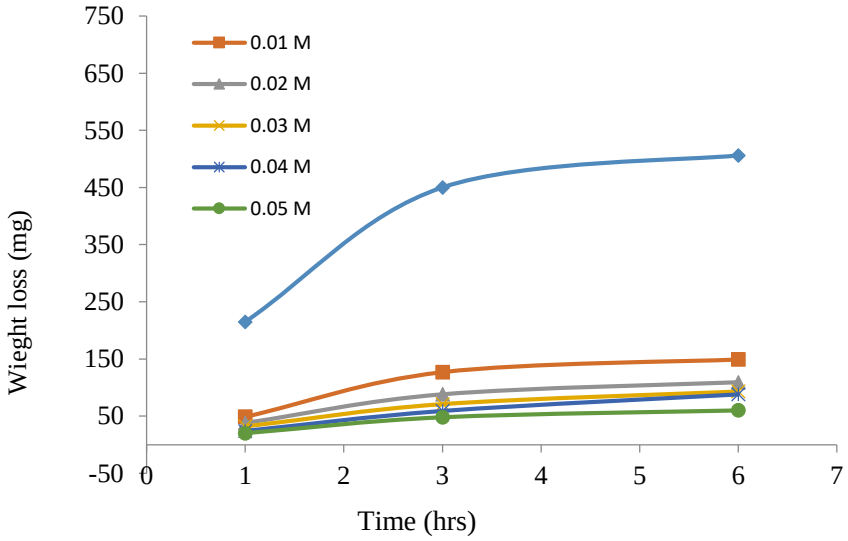


**Figure 8.** Weight loss of N-80 at different times at 30±2°C.

**Table 5.** Results of weight loss method at different times at 70±2°C.

| Time | 1 hr. | | | 3 hrs. | | | 6 hrs. | | |
|---|---|---|---|---|---|---|---|---|---|
| **Conc., mol·L$^{-1}$** | ***WL*, mg** | **%*IE*** | **θ** | ***WL*, mg** | **%*IE*** | **θ** | ***WL*, mg** | **%*IE*** | **θ** |
| 0.5 HCl | 311 | – | – | 591 | – | – | 669 | – | – |
| 0.01 | 79 | 74.59 | 0.7459 | 188 | 68.18 | 0.6818 | 221 | 66.96 | 0.6696 |
| 0.02 | 65 | 79.09 | 0.7909 | 169 | 71.40 | 0.7140 | 196 | 70.70 | 0.7070 |
| 0.03 | 54 | 82.63 | 0.8263 | 148 | 74.95 | 0.7495 | 177 | 73.54 | 0.7354 |
| 0.04 | 43 | 86.17 | 0.8617 | 128 | 78.34 | 0.7834 | 151 | 77.42 | 0.7742 |
| 0.05 | 39 | 87.45 | 0.8745 | 99 | 83.24 | 0.8324 | 123 | 81.61 | 0.8161 |

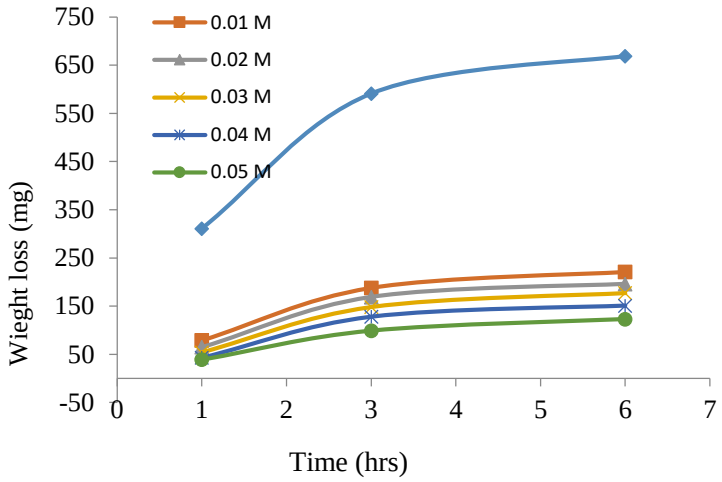


**Figure 9.** Weight loss of N-80 at different times at 70±2°C.

### *3.5. Adsorption behavior of the inhibitor*

From the results of the weight loss method previously mentioned, the N-80 surface covered by inhibitor molecules of SHBA increases considerably whenever the inhibitor concentration increases, indicating the adsorption on the carbon steel surface is larger. Several adsorption isotherms were assessed, such as Frumkin, Temkin, Langmuir, and Freundlich isotherms, where the best fit obtained is a Langmuir adsorption isotherm. Langmuir adsorption by plotting $C_{inh}/\theta$ *versus* $C_{inh}$ was determined for various concentrations of inhibitor, where straight lines have been given at correlation coefficient is close to one. The best fit of correlation coefficient are $r^2$=0.999829 and $r^2$=0.999717 at 303 K and 343 K, respectively. Also, it can be concluded that concentration is directly proportional to $C_{inh}/\theta$ and the relation is a good linear as shown in Figure 10, suggesting the Langmuir model is suitable to describe the adsorption process of inhibitor molecules on the surface [12, 45].

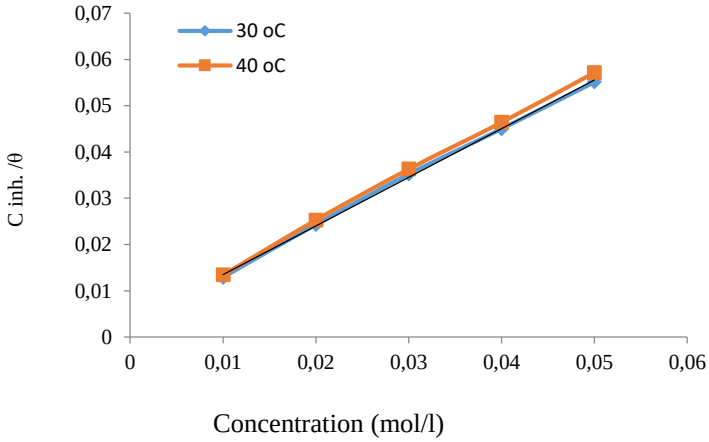


**Figure 10.** Langmuir adsorption of inhibitor on N-80 surface at optimum efficiency.

### *3.6. Results analysis of Fermi levels and Monte Carlo simulation*

Understanding how molecules adsorb onto a metal surface is complex because the active centers of the molecules and the metal surface can exhibit different adsorption behaviors. Therefore, to identify adsorption sites on the Fe surface and analyze its surface inhibition mechanism, the Fermi level and Monte Carlo (MC) were studied [46]. The adsorption of SHBA on the iron surface is shown in Figure 11 from both top and side views. Notably, after 300 ps at 273 K, the inhibitor molecules moved closer to the Fe (111) surface and aligned in a nearly flat position, parallel to the Fe surface through all their oxygen and nitrogen atoms. The orientation of the SHBA molecule confirms that electron donation from the active centers, specifically the O and N orbitals, has protected the iron surface from corrosion [47, 48]. The *HOMO* energy of SHBA is (–6.022 eV), which is higher than the Fermi level energy at –28.188 eV (–0.8756 Ha), as shown in Figure 12, indicating strong adsorption capability on the iron surface, which supports the MC results. Furthermore, it was observed that no band exceeded the Fermi level, indicating metallic properties due to the absence of overlap between the top of the valence band and the bottom of the conduction band (Figure 12) [3, 49, 50]. If the $\Delta E_{\text{back-donation}}$ of the SHBA inhibitor is negative and the hardness is positive, this indicates that charge transfer to the molecule is followed by back-donation from the molecule. Consequently, stabilization may occur between the inhibitory molecules and the metal surface [51]. Table 5 presents the results of the SHBA analysis, showing that the hardness was 0.892 eV ($\eta>0$) and the $\Delta E_{\text{back-donation}}$ was –0.223 eV ($\Delta E<0$); thus, SHBA molecules might stabilize on the surface of Fe. The dipole moment ($\mu$), which indicates the negative value of electronegativity ($\mu=-\chi$), is useful for predicting the direction of a corrosion inhibition process and measuring the polarity of a covalent bond. It describes the inhibitor's polarity related to the electron distribution in molecules. Literature indicates that a low dipole moment causes inhibitor molecules to accumulate on the metallic surface, leading to adsorption [52–54]. The dipole moment value of SHBA is low at –5.130 Debye. Therefore, it can be concluded that SHBA will favor the accumulation of its molecules on the N-80 surface. The Electron Potential Surface (EPS) is a key feature for identifying reactive regions in molecules. Red areas indicate more negative regions (electrophilic attack), while blue areas indicate more positive sites (nucleophilic attack). Green, pink, and yellow regions represent intermediate electrostatic potential. The SHBA molecules showed negative potential charges at the atoms $O_5$ (0.491e), $O_6$ (–0.914e), $O_{11}$ (–0.634e), $O_{21}$ (–0.799e), $O_{29}$ (–0.336e), $O_{44}$ (–0.442e), $N_9$ (–0.521e), $N_{33}$ (–0.422e), $C_{38}$ (–0.447e), $C_{45}$ (–0.274e), $Br_{137}$ (–0.888e), and $Br_{138}$ (–0.878e), indicating potential sites for electrophilic attack. Positive charges appeared on hydrogen and carbon atoms, with high values at $C_3$ (0.744e), $H_{53}$ (0.801e), $H_{59}$ (0.609e), $H_{88}$ (0.517e), and $H_{103}$ (0.422e), indicating potential sites for nucleophilic attack, as shown in Figure 13 and Table 6. Therefore, EPS analysis enabled a systematic evaluation of the reactive zones of SHBA, with various color contrasts that facilitate understanding how molecules interact on the surface of Fe [3, 26].

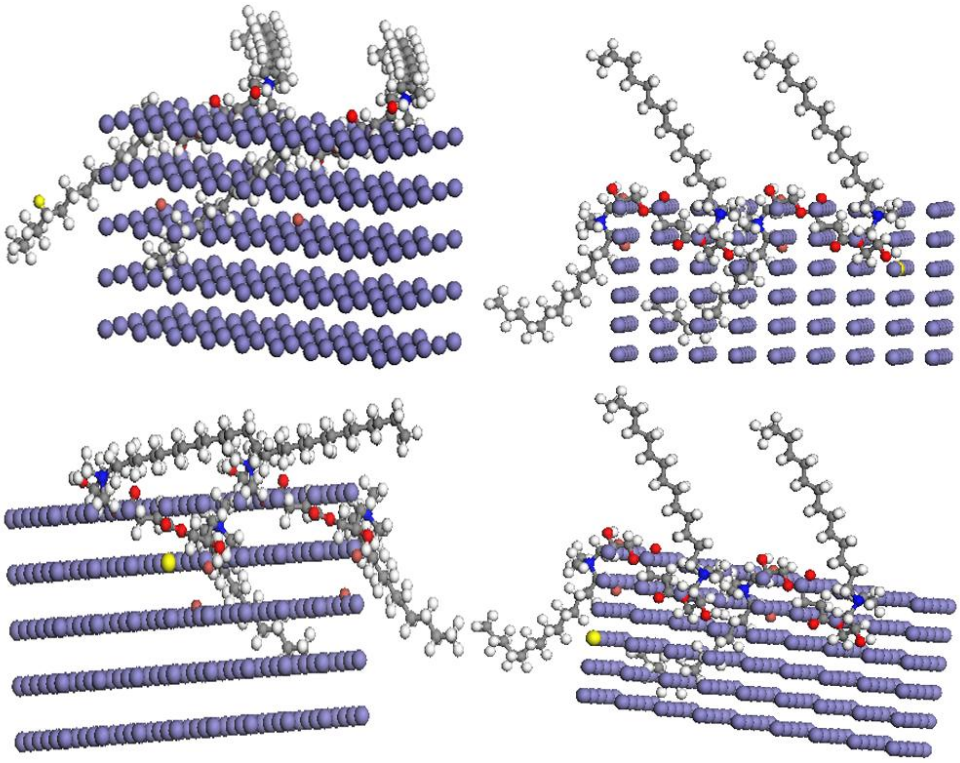

**Figure 11.** Monte Carlo of the SHBA molecules on the Fe (111) surface; the left is the side view, and the right is the top view.

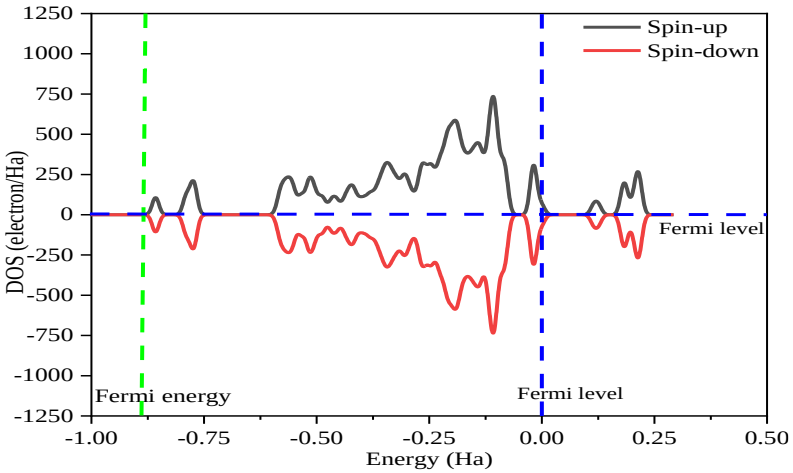


**Figure 12.** Fermi energy and Fermi level of the SHBA molecule by DMol3 software.

**Table 6.** Charges of all SHBA atoms via EPS.

| Atoms | Charge, e | *V*(*r*), au | Atoms | Charge, e | *V*(*r*), au | Atoms | Charge, e | *V*(*r*), au |
|---|---|---|---|---|---|---|---|---|
| C(1) | 0.112 | −3.1413 | C(48) | −0.111 | −14.7216 | H(95) | 0.104 | −1.7356 |
| C(2) | −0.057 | −6.0339 | C(49) | −0.100 | −13.0296 | H(96) | 0.000 | −3.7157 |

| Atoms | Charge, e | *V*(*r*), au | Atoms | Charge, e | *V*(*r*), au | Atoms | Charge, e | *V*(*r*), au |
|---|---|---|---|---|---|---|---|---|
| C(3) | 0.744 | −7.9001 | C(50) | 0.001 | −11.0304 | H(97) | 0.102 | −3.7648 |
| C(4) | −0.091 | −4.7461 | C(51) | 0.111 | −14.9761 | H(98) | 0.019 | −3.7176 |
| O(5) | −0.491 | −3.9110 | C(52) | 0.101 | −3.1079 | H(99) | 0.105 | −7.6253 |
| O(6) | −0.914 | −1.3490 | H(53) | 0.801 | −5.9991 | H(100) | 0.019 | −7.7025 |
| C(7) | 0.012 | −1.2206 | H(54) | 0.182 | −9.1160 | H(101) | 0.081 | −2.3994 |
| C(8) | 0.011 | −9.2398 | H(55) | 0.217 | −19.1702 | H(102) | 0.000 | −2.3401 |
| N(9) | −0.521 | −8.0152 | H(56) | 0.102 | −16.1052 | H(103) | 0.422 | −2.3549 |
| C(10) | −0.116 | −11.7632 | H(57) | 0.172 | −17.1032 | H(104) | 0.110 | −2.1910 |
| O(11) | −0.634 | −9.1192 | H(58) | 0.100 | −2.70092 | H(105) | 0.121 | −1.0901 |
| C(12) | 0.111 | −16.9907 | H(59) | 0.609 | −11.3024 | H(106) | 0.116 | −2.7528 |
| C(13) | −0.090 | −10.1921 | H(60) | 0.114 | −13.9212 | H(107) | 0.110 | −2.1856 |
| C(14) | −0.044 | −7.1222 | H(61) | 0.101 | −17.0261 | H(108) | 0.001 | −12.753 |
| C(15) | −0.107 | −1.5439 | H(62) | 0.110 | −11.6304 | H(109) | 0.111 | −12.632 |
| C(16) | −0.019 | −1.0991 | H(63) | 0.103 | −11.9761 | H(110) | 0.009 | −12.772 |
| C(17) | −0.135 | −9.0954 | H(64) | 0.120 | −7.1179 | H(111) | 0.005 | −12.401 |
| C(18) | 0.000 | −5.1241 | H(65) | 0.120 | −7.0991 | H(112) | 0.091 | −11.756 |
| C(19) | −0.109 | −19.3041 | H(66) | 0.102 | −7.1160 | H(113) | 0.011 | −9.0557 |
| C(20) | −0.114 | −15.1751 | H(67) | 0.111 | −5.1170 | H(114) | 0.112 | −22.756 |
| O(21) | −0.799 | −10.3156 | H(68) | 0.091 | −5.1252 | H(115) | 0.122 | −1.7557 |
| C(22) | −0.102 | −11.3071 | H(69) | 0.007 | −8.1232 | H(116) | 0.103 | −8.7698 |
| C(23) | −0.022 | −11.7921 | H(70) | 0.080 | −2.0914 | H(117) | 0.109 | −8.7186 |
| C(24) | −0.420 | −1.9962 | H(71) | 0.041 | −1.0786 | H(118) | 0.104 | −8.6953 |
| C(25) | −0.226 | −8.7563 | H(72) | 0.005 | −8.1171 | H(119) | 0.132 | −22.725 |
| C(26) | 0.000 | −3.7983 | H(73) | 0.114 | −8.0991 | H(120) | 0.101 | −2.3994 |
| C(27) | −0.108 | −11.612 | H(74) | 0.082 | −8.1117 | H(121) | 0.101 | −2.3901 |
| C(28) | −0.061 | −17.7561 | H(75) | 0.202 | −4.1971 | H(122) | 0.032 | −2.3859 |
| O(29) | −0.336 | −4.7255 | H(76) | 0.021 | −9.1924 | H(123) | 0.108 | −22.110 |
| C(30) | 0.012 | −11.1697 | H(77) | 0.006 | −9.1193 | H(124) | 0.018 | −11.090 |
| O(31) | −0.045 | −7.3042 | H(78) | 0.002 | −21.344 | H(125) | 0.101 | −13.728 |
| C(32) | −0.026 | −2.3159 | H(79) | 0.092 | −17.333 | H(126) | 0.133 | −13.856 |
| N(33) | −0.422 | −16.3102 | H(80) | 0.122 | −2.3124 | H(127) | 0.102 | −11.753 |

| Atoms | Charge, e | *V*(*r*), au | Atoms | Charge, e | *V*(*r*), au | Atoms | Charge, e | *V*(*r*), au |
|---|---|---|---|---|---|---|---|---|
| C(34) | −0.012 | −12.3207 | H(81) | 0.051 | −11.3113 | H(128) | 0.211 | −10.692 |
| O(35) | −0.071 | −6.7252 | H(82) | 0.105 | −11.7235 | H(129) | 0.105 | −12.732 |
| C(36) | 0.003 | −6.7622 | H(83) | 0.105 | −13.7262 | H(130) | 0.111 | −12.501 |
| C(37) | 0.122 | −2.8981 | H(84) | 0.104 | −6.2728 | H(131) | 0.001 | −12.256 |
| C(38) | −0.447 | −16.7832 | H(85) | 0.139 | −1.2324 | H(132) | 0.117 | −3.7597 |
| C(39) | 0.540 | −2.7182 | H(86) | 0.002 | −15.0914 | H(133) | 0.114 | −3.7698 |
| C(40) | 0.341 | −10.6151 | H(87) | 0.022 | −17.0786 | H(134) | 0.172 | −3.7486 |
| C(41) | 0.410 | −1.7575 | H(88) | 0.517 | −17.1171 | H(135) | 0.108 | −8.6853 |
| C(42) | 0.114 | −9.3449 | H(89) | 0.105 | −21.0991 | H(136) | 0.021 | −22.025 |
| C(43) | −0.102 | −12.2311 | H(90) | 0.112 | −2.1377 | Br(137) | −0.888 | −22.025 |
| O(44) | −0.442 | −6.3543 | H(91) | 0.004 | −6.1271 | Br(138) | −0.878 | −21.094 |
| C(45) | −0.274 | −2.3374 | H(92) | 0.009 | −6.9824 | | | |
| C(46) | −0.006 | −14.7170 | H(93) | 0.104 | −5.1099 | | | |
| C(47) | −0.085 | −12.7211 | H(94) | 0.091 | −13.224 | | | |

**Table 7.** Electronic characteristics of SHBA by DMol3 software.

| Electronic Characteristics | Values |
|---|---|
| *HOMO* | –6.022 eV |
| *LUMO* | –4.238 eV |
| Energy gap ($\Delta E_{gap}$) | 1.784 eV |
| $\Delta E_{back\text{-}donation}$ | –0.223 eV |
| Softness (*s*) | 1.121 eV |
| Hardness (η) | 0.892 eV |
| Ionization energy ($I_E$) | 6.022 eV |
| Electronegativity (χ) | 5.130 eV |
| Dipole moment (μ) | –5.130 Debye |
| Fermi energy of SHBA | –0.8756 Ha |

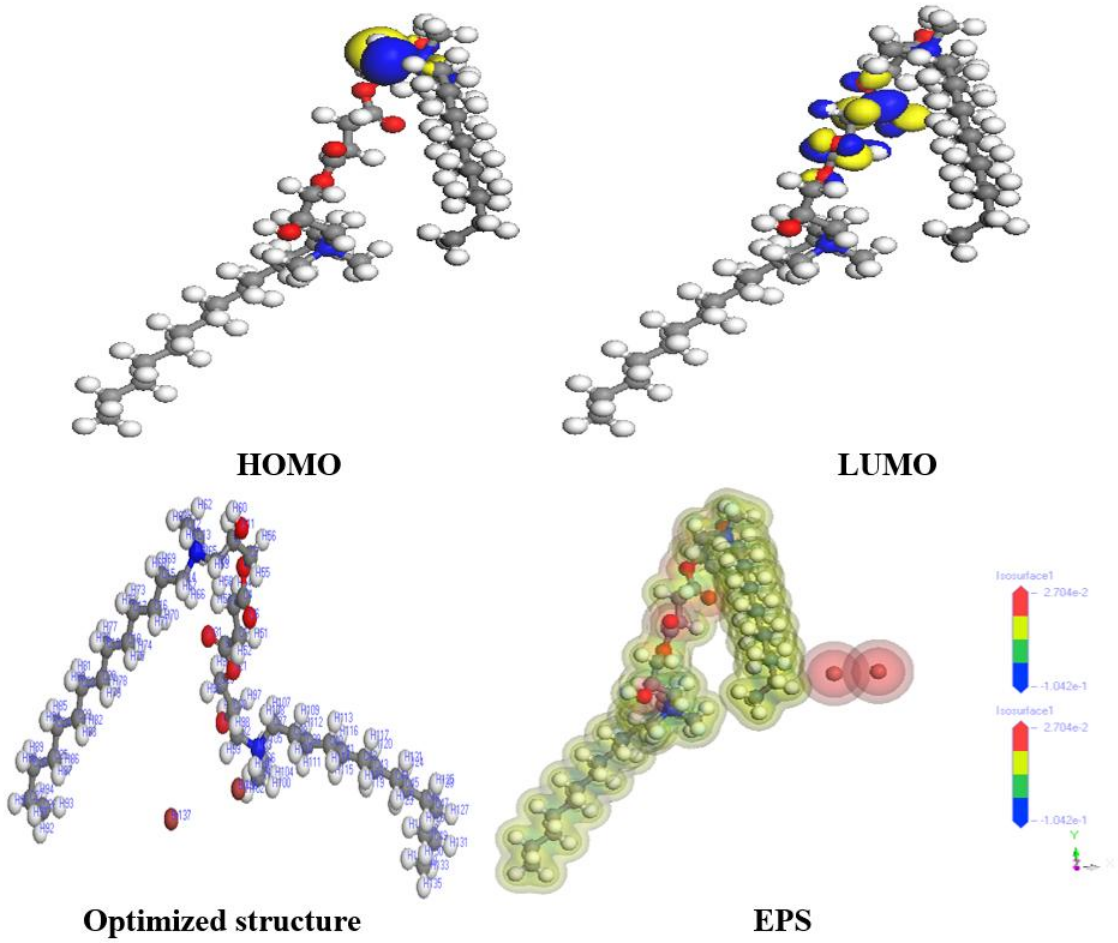


**Figure 13.** *HOMO*, *LUMO*, EPS, and optimized structure of the SHBA molecule.

## 4. Conclusions

The SHBA compound was synthesized to study its role as an iron corrosion inhibitor. Results showed that SHBA is highly effective in 0.5 M HCl. The highest inhibition efficiencies, 93.63%, 93.04%, and 95.38% using the EIS, PP, and EDX techniques, respectively, have been recorded. As SHBA concentration increases, the inhibition efficiency increases. PP analysis indicates that SHBA is a mixed-type inhibitor. The ability of SHBA to donate electrons to the iron surface was confirmed by Fermi level studies and Monte Carlo simulations, demonstrating its strong anticorrosive activity. The experimental inhibition efficiency closely aligns with the quantum characteristics of SHBA. The oxygen, nitrogen, bromine, and some carbon atoms in SHBA carry negative charges, making them sites for electrophilic attack. Several carbon and hydrogen atoms have positive charges, indicating potential sites for nucleophilic attack. *HOMO* energy exceeds the Fermi energy, demonstrating a strong ability to adsorb onto the carbon steel surface. Analysis with the EDX technique supports and strengthens the results from the EIS and PP methods. The PZC values are lower than the OCP values, indicating that the N-80 surface is positively charged. These

conclusions not only enhance our understanding of SHBA's role as an inhibitor but also guide corrosion protection research, especially in real-world applications.

## References


1. M.J. Meften and A.A. Kadhim, Synthesis of 5-benzyl-5-((5-nitropyridin-3-yl) methyl) 1,3,5-dithiazinan-5-ium through one-pot reactions, characterization, and study as a corrosion retardant in high salinity oil fields, *J. Basrah Res. (Sci.)*, 2023, **49**, no. 2, 140–163. doi: 10.56714/bjrs.49.2.12
2. A.A. Alamiery, Schiff bases as corrosion inhibitors: A mini-review, *J. Mater. Eng.*, 2024, **02**, no. 3, 170–185. doi: 10.61552/JME.2024.03.003
3. M.J. Meften, A.A. Kadhim, A.S. Abdulnabi and J.M.K. Al-zyadi, Electrochemical appraisal of gemini surfactant as an inhibitor to reduce corrosion: simulation study to relate the inhibition efficiency with the electronic characteristics, *Int. J. Corros. Scale Inhib.*, 2025, **14**, no. 1, 38–60. doi: 10.17675/2305-6894-2025-14-1-3
4. R.M. Kubba, M.A. Mohammed and L.S. Ahamed, DFT calculations and experimental study to inhibit carbon steel corrosion in saline solution by quinoline-2-one derivative, *Baghdad Sci. J.*, 2021, **18**, no. 1, 113–123. doi: 10.21123/bsj.2021.18.1.0113
5. H. Zheng, Y. Liu, Y. Zhou, D. Zhao, D. Wang, L. Yun, D. Zhang and L. Zhang, Improved photocathodic protection performance of g-$C_3N_4$/rGO/ZnS for 304 stainless steel, *J. Phys. Chem. Solids*, 2020, **148**, 109672. doi: 10.1016/j.jpcs.2020.109672
6. L. Guo, X. Ren, Y. Zhou, S. Xu and Y. Gong, Monte Carlo simulations of corrosion inhibition of copper by two Schiff bases, *Int. Conf. Mater., Environ. Biol. Eng.*, 2015, 622–625. doi: 10.2991/mebe-15.2015.143
7. J.M. Castillo-Robles, E.F. Martins, P. Ordejón and I. Cole, Molecular modeling applied to corrosion inhibition: a critical review, *Mater. Degrad.*, 2024, **8**, no. 72, 1–20. doi: 10.1038/s41529-024-00478-2
8. S. Hadisaputra, A.A. Purwoko, A. Hakim, N. Prasetyo and S. Hamdiani, Corrosion inhibition properties of phenyl phthalimide derivatives against carbon steel in the acidic medium: DFT, MP2, and Monte Carlo simulation studies, *ACS Omega*, 2022, **7**, 33054–33066. doi: 10.1021/acsomega.2c03091
9. J. Fang and J. Li, Quantum chemistry study on the relationship between molecular structure and corrosion inhibition efficiency of amides, *J. Mol. Struct.*, 2002, **593**, 179–185. doi: 10.1016/S0166-1280(02)00316-0
10. T. Arslan, F. Kandemirli, E.E. Ebenso, I. Love and H. Alemu, Quantum chemical studies on the corrosion inhibition of some sulphonamides on mild steel in acidic medium, *Corros. Sci.*, 2009, **51**, no. 1, 35–47. doi: 10.1016/j.corsci.2008.10.016
11. M.J. Meften, W.A. Radhi and A.N. Abulhail, Molecular structure and electronic characteristics study of imidazole and dioxol derivatives as corrosion inhibitors. A quantum methodology investigation, *Basrah J. Sci.*, 2018, **36**, no. 1, 1–29. doi: 10.29072/basjs.2018302

12. M.J. Meften, Gemini surfactant performance evaluation as inhibitive action of PAPM for treatment of AISI steel corrosion and studying temperatures influence in acidic medium, *Univ. Thi-Qar J. Sci*., 2019, **7**, no. 1, 103–112. doi: 10.32792/utq/utjsci/v7i1.260
13. Q. Zhang, Z. Gao, F. Xu and X. Zou, Adsorption and corrosion inhibitive properties of gemini surfactants in the series of hexanediyl-1,6-bis-(diethyl alkyl ammonium bromide) on aluminium in hydrochloric acid solution, *Colloids Surf., A.*, 2011, **380**, 191–200. doi: 10.1016/j.colsurfa.2011.02.035
14. M. Yadav, D. Behera and U. Sharma, Nontoxic corrosion inhibitors for N80 steel in hydrochloric acid, *Arabian J. Chem*., 2016, **9**, 1487–1495. doi: 10.1016/j.arabjc.2012.03.011
15. N.Z. Rajab, *Synthesis, characterization, and study of Gemini surfactants as De-Emulsifier for treatment of water in crude oil (W/O) emulsions*, Ph.D Thesis, College of Education for Pure Sciences, University of Basrah, Iraq, 2014.
16. A.S. Fouda and H.M. Elabbasy, Corrosion inhibition effect of methanol extract of *Nerium oleander* on copper in nitric acid solutions, *Int. J. Electrochem. Sci*., 2019, **14**, 6884–6901. doi: 10.20964/2019.07.31
17. S. John and A. Joseph, Electroanalytical surface morphological and theoretical studies on the corrosion inhibition behavior of different 1,2,4-triazole precursors on mild steel in 1 M hydrochloric acid, *Mater. Chem. Phys*., 2012, **133**, no. 2, 1083–1091. doi: 10.1016/j.matchemphys.2012.02.020
18. R. Ganjoo, S. Sharma, P.K. Sharma, O. Dagdag, A. Berisha, E.E. Ebenso, A. Kumar and C. Verma, Coco Monoethanolamide Surfactant as a Sustainable Corrosion Inhibitor for Mild Steel: Theoretical and Experimental Investigations, *Molecules*, 2023, **28**, no. 4, 1–24. doi: 10.3390/molecules28041581
19. S.A. Ali, M.A.J. Mazumder, M.K. Nazal and H.A. Al-Muallem, Assembly of succinic acid and isoxazolidine motifs in a single entity to mitigate $CO_2$ corrosion of mild steel in saline media, *Arabian J. Chem*., 2020, **13**, 242–257. doi: 10.1016/j.arabjc.2017.04.005
20. H.M. Elabbasy, Investigation of *Withania somnifera* extract as corrosion inhibitor for copper in nitric acid solutions, *Int. J. Electrochem. Sci*., 2019, **14**, no. 6, 5355–5372. doi: 10.20964/2019.06.23
21. G.G. Sánchez, N.V. Likhanova, P. Lozada, J.A. Morales, N. Nava, O.O. Xometl, I.V. Lijanova and G. Corro, Electrochemical, surface and 1018-steel corrosion product characterization in sulfuric acid with new imidazole-derived inhibitors, *Int. J. Electrochem. Sci*., 2019, **14**, no. 9, 9255–9272. doi: 10.20964/2019.09.65
22. M.J. Meften, N.Z. Rajab and M.T. Finjan, Synthesis of new heterocyclic compound used as corrosion inhibitor for crude oil pipelines, *Am. Sci. Res. J. Eng. Technol. Sci*., 2017, **27**, no 1, 419–437.
23. M.Y. Chaudhary, S. Yadav, P. Bansal, Y.S. Sharma, M. Gautam, C. Chandra, A.K. Kalra and M. Gupta, Towards sustainable corrosion inhibition: A combined experimental and computational study of ethyl triphenyl phosphonium iodide on

aluminum in acidic medium, *Sustainable Chem. Environ.*, 2025, **9**, 100221. doi: 10.1016/j.scenv.2025.100221
24. M.J. Meften, Preparation of novel compounds, characterization, and studying experimentally and theoretically as inhibitors through thermodynamic and quantum chemistry, *Eur. J. Chem.*, 2017, **8**, no. 3, 229–239. doi: 10.5155/eurjchem.8.3.229-239.1589
25. M. Adardour, M. Lasri, M.A. Lahcen, M. Maatallah, R. Idouhli, M.M. Alanazi, S. Lahmidi, A. Abouelfida, J.T. Mague and A. Baouid, Exploring the efficacy of benzimidazolone derivatives as corrosion inhibitors for copper in a 3.5 wt.% NaCl solution: A comprehensive experimental and theoretical investigation, *Molecules*, 2023, **28**, no. 19, 6948. doi: 10.3390/molecules28196948
26. N.O. Obi-Egbedi and I.B. Obot, Xanthione: A new and effective corrosion inhibitor for mild steel in sulphuric acid solution, *Arabian J. Chem.*, 2013, **6**, no. 2, 211–223. doi: 10.1016/j.arabjc.2010.10.004
27. A. Toghan, M. Khairy, M. Huang and A.A. Farag, Electrochemical, chemical and theoretical exploration of the corrosion inhibition of carbon steel with new imidazole carboxamide derivatives in an acidic environment, *Int. J. Electrochem. Sci.*, 2023, **18**, no. 3, 100072. doi: 10.1016/j.ijoes.2023.100072
28. C.U. Dueke-Eze, N.A. Madueke, N.B. Iroha, N.J. Maduelosi, L.A. Nnanna, V.C. Anadebe and A.A. Chokor, Adsorption and inhibition study of *N*-(5-methoxy-2-hydroxybenzylidene) isonicotinohydrazide Schiff base on copper corrosion in 3.5% NaCl, *Egypt. J. Pet.*, 2022, **31**, no. 2, 31–37. doi: 10.1016/j.ejpe.2022.05.001
29. L.B. Furtado, G.B. Leoni, R.C. Nascimento, P.H.C. Santos, F.J.F.S. Henrique, M.O.C. Guimarães and S.L.C. Brasil, Experimental and theoretical studies of Tailor-made Schiff bases as corrosion inhibitors for carbon steel in HCl, *Mater. Res.*, 2023, **26**, 1–18. doi: 10.1590/1980-5373-MR-2022-0398
30. A. Toghan, A. Fawzy, A.I. Alakhras, M.M.S. Sanad, M. Khairy and A.A. Farag, Correlating experimental with theoretical studies for a new ionic liquid for inhibiting corrosion of carbon steel during oil well acidification, *Metals*, 2023, **13**, no. 5, 862. doi: 10.3390/met13050862
31. N.A. Othman, M.M. Ali, N.S. Samsi, F. Salim, D. Panuh, M.K. Yaakob, Z. Embong, A.S. Sauri, N.N.C. Isa and N.Z.N. Hashim, Environmentally conscience corrosion inhibitors for mild steel in corrosive hydrochloric acid solution by *Uncaria cordata* extract: experimental and theoretical studies, *J. Adhes. Sci. Technol.*, 2023, **37**, no. 23, 3419–3447. doi: 10.1080/01694243.2023.2196905
32. K. Azizollah and S. Ahmadi, Synergistic effect between oleic imidazoline and 2 mercaptobenzimidazole for increasing the corrosion inhibition performance in carbon steel samples, *Iran. J. Chem. Chem. Eng.*, 2023, **42**, no. 1, 1–16. doi: 10.30492/ijcce.2022.546098.5091

33. L. Feng, C. Yin, H. Zhang, Y. Li, X. Song, Q. Chen and H. Liu, Cationic Gemini surfactants with a bipyridyl spacer as corrosion inhibitors for carbon steel, *ACS Omega*, 2018, **3**, no. 12, 18990–18999. doi: 10.1021/acsomega.8b03043
34. H. Elmsellem, K. Karrouchi, A. Aouniti, B. Hammouti, S. Radi, J. Taoufik, M. Ansar, M. Dahmani, H. Steli and B. El Mahi, Theoretical prediction and experimental study of 5-methyl-1*H*-pyrazole-3 carbohydrazide as a novel corrosion inhibitor for mild steel in 1.0 M HCl, *Der Pharma Chem*., 2015, **7**, no. 10, 237–245.
35. S. Chitra, K. Parameswari and A. Selvaraj, Dianiline schiff bases as inhibitors of mild steel corrosion in acid media, *Int. J. Electrochem. Sci*., 2010, **5**, no. 11, 1675–1697. doi: 10.1016/S1452-3981(23)15421-6
36. S.A. Abd El-Maksoud, F.I. El-Dossoki, M. Abd-Elhamed and A.A. Farag, Some new synthesized gemini cationic surfactants as corrosion inhibitors for carbon steel in hydrochloric acid solution, *J. Bio Tribo Corros*., 2023, **9**, no. 71, 1–51. doi: 10.21203/rs.3.rs-2679512/v1
37. S.N. Dalhatu, K.A. Modu, A.A. Mahmoud, Z.U. Zango, A.B. Umar, F. Usman, J.O. Dennis, A. Alsadig, K.H Ibnaouf and O.A. Aldaghri, *L*-Arginine grafted chitosan as corrosion inhibitor for mild steel protection, *Polymers*, 2023, **15**, no. 2, 1–14. doi: 10.3390/polym15020398
38. S. Fu, X. Yang, Y. Peng, Q. Wang, Q. Sun, J. Zhang, X. Wang, Z. Liang and J. Li, Corrosion behaviors of tetrasodium iminodisuccinate (IDS) as an environmentally friendly inhibitor: experimental and theoretical studies, *Coatings*, 2023, **13**, no. 3, 1–7. doi: 10.3390/coatings13030613
39. S. Tanwer and S.K. Shukla, Cefuroxime: A Potential corrosion inhibitor for mild steel in sulphuric acid medium, *Prog. Color, Color. Coat*., 2023, **16**, no. 2, 125–138. doi: 10.30509/pccc.2022.166974.1165
40. A.E. Vázquez, M.A.C. Robles, G.E.N. Silva, F.J.R. Gómez, M.P. Pardavé, L.L. Romero, D.Á. Beltrán and D.P. Martínez, Carbohydrates as corrosion inhibitors of API 5L X70 steel immersed in acid medium, *Int. J. Electrochem. Sci*., 2019, **14**, 9206–9220. doi: 10.20964/2019.09.57
41. M.J. Meften and A.S. Abdulnabi, Synthesis of a new heterocyclic compound through domino reactions, identification, and study them as corrosion inhibitors for carbon steel in brine water, *Int. J. Eng. Tech. Res*., 2014, **2**, no. 12, 7–11.
42. L.L. Schramm, Surfactants fundamentals and applications in the petroleum industry, 1st ed., Cambridge University, U.K, 2000.
43. R. Saratha and V.G. Vasudha, *Emblica officinalis* (*Indian gooseberry*) leaves extract as corrosion inhibitor for mild steel in 1 N HCl medium, *J. Chem*., 2010, **7**, no. 3. doi: 10.1155/2010/162375
44. V.A. Panchal, A.S. Patel, P.T. Trivedi and N.K. Shah, Corrosion inhibition of Al-Mg alloy in hydrochloric acid using benzylamine-*N*-(*p*-methoxy benzylidene), *J. Mater. Environ. Sci*., 2012, **3**, no. 2, 360–373.

45. M. Abdallah, I.A. Zaafarany and B.A.A. Jahdalya, Corrosion inhibition of zinc in hydrochloric acid using some antibiotic drugs, *J. Mater. Environ. Sci*., 2016, **7**, no. 4, 1107–1118.
46. A. Toghan, A. Fawzy, A.I. Alakhras, M.M.S. Sanad, M. Khairy and A.A. Farag, Correlating experimental with theoretical studies for a new ionic liquid for inhibiting corrosion of carbon steel during oil well acidification, *Metals*, 2023, **13**, no. 5, 862. doi: 10.3390/met13050862
47. C. Verma, H. Lgaz, D.K. Verma, E.E. Ebenso, I. Bahadur, and M.A. Quraishi, Molecular dynamics and Monte Carlo simulations as powerful tools for study of interfacial adsorption behavior of corrosion inhibitors in aqueous phase: A review, *J. Mol. Liq*., 2018, **260**, 99–120. doi: 10.1016/j.molliq.2018.03.045
48. O.E. Oyeneyin, N.D. Ojo, N. Ipinloju, E.B. Agbafa and A.V. Emmanuel, Investigation of the corrosion inhibition potentials of some 2-(4-(substituted) arylidene)-1*H*-indene-1,3-dione derivatives: density functional theory and molecular dynamics simulation, *Beni-Suef. Univ. J. Basic. Appl. Sci*., 2022, **11**, no. 132, 1–14. doi: 10.1186/s43088-022-00313-0
49. A.K. Kushwaha, M.R. Sahoo, M. Ray, D. Das, S. Nayak, A. Maity, K. Sarkar, A.N. Bhagat, A.R. Pal, T.K. Rout and S.K. Nayak, Functional pyromellitic diimide as a corrosion inhibitor for galvanized steel: An atomic-scale engineering, *ACS Omega*, 2022, **7**, no. 31, 27116–27125. doi: 10.1021/acsomega.2c01299
50. H.A. Aisha, C. Abdelkarim, M.A. Jamilah, A.A. Wesam, A.N. Ehteram, A.A. Azza and G.K. Young, Development of natural plant extracts as sustainable inhibitors for efficient protection of mild steel: experimental and first-principles multi-level computational methods, *Materials*, 2022, **15**, no. 23, 8688. doi: 10.3390/ma15238688
51. P. Udhayakalaa, T.V. Rajendiranb and S. Gunasekaranc, Theoretical evaluation of corrosion inhibition performance of some triazole derivatives, *J. Adv. Sci. Res*., 2012, **3**, no. 2, 71–77. Link
52. A.M. Al-Sabagh, M.N. Notaila, A.F. Ahmed, A.M. Mohamed, M.F.E. Abdelmonem and M. Tahany, Structure effect of some amine derivatives on corrosion inhibition efficiency for carbon steel in acidic media using electrochemical and quantum theory methods, *Egypt. J. Pet*., 2013, **22**, 101–116. doi: 10.1016/j.ejpe.2012.09.004
53. M.N. Paulin, S. Drissa, T. Albert, Y. Assemian, K.A. Henri and D. Donourou, Thermodynamic and quantum chemistry characterization of adsorption of 2-hydroxymethylbenzimidazole (HMBI) and 2-thiomethyl benzimidazole (TMBI) during copper corrosion inhibition in 1M nitric acid, *J. Soc. Ouest-Afr. Chim*., 2010, **30**, 49–58.
54. P. Nithya, S. Rameshkumar and A. Sankar, Experimental and theoretical studies on the corrosion inhibition performance of a synthesized Schiff base on the corrosion of mild steel in HCl solution, *Chem. Sci. Rev. Lett*., 2017, **6**, no. 21, 20–30.

♦ ♦ ♦